PAPER

Spin polarized bound states in the continuum in open Aharonov–Bohm rings with the Rashba spin–orbit interaction

To cite this article: Evgeny N Bulgakov and Almas F Sadreev 2016 *J. Phys.: Condens. Matter* **28** 265301

IOP Publishing Journal of Physics: Condensed Matter
J. Phys.: Condens. Matter **28** (2016) 265301 (12pp) doi:10.1088/0953-8984/28/26/265301

Spin polarized bound states in the continuum in open Aharonov–Bohm rings with the Rashba spin–orbit interaction

Evgeny N Bulgakov[1,2] **and Almas F Sadreev**[1]

[1] Kirensky Institute of Physics, Academy of Sciences, 660036 Krasnoyarsk, Russia
[2] Siberian State Aerospace University, Krasnoyarsk 660014, Russia

E-mail: almas@tnp.krasn.ru

Received 16 March 2016, revised 22 April 2016
Accepted for publication 22 April 2016
Published 11 May 2016

Abstract

We consider the trapping of electrons with a definite spin polarization by bound states in the continuum (BSC) in the open Aharonov–Bohm rings in the presence of the Rashba spin–orbit interaction (RSOI). Neglecting the Zeeman term we show the existence of BSCs in the one-dimensional ring when the eigenstates of the closed ring are doubly degenerate. With account of the Zeeman term BSCs occur only at the points of threefold degeneracy. The BSCs are found in the parametric space of flux and RSOI strength in close pairs with opposite spin polarization. Thereby the spin polarization of electrons transmitted through the ring can be altered by minor variation of magnetic or electric field at the vicinity of these pairs. Numerical simulations of the two-dimensional open ring show similar results for the BSCs. Encircling the BSC points in the parametric space of the flux and the RSOI constant gives rise to a geometric phase.

Keywords: Aharonov–Bohm ring, Rashba spin–orbit interaction, bound states in the continuum

(Some figures may appear in colour only in the online journal)

1. Introduction

If waveguides are attached to a quantum dot (QD) the bound states of the QD residing in the propagation band become resonant states with finite resonant widths. There could be however an exception to this widely accepted rule [1, 2]. According to Friedrich and Wintgen [3, 4] if two resonances pass each other as a function of continuous parameter one of the states can acquire zero resonance width. Thus, this resonance state becomes a bound state in the continuum (BSC). The Friedrich–Wintgen mechanism of destructive interference of two resonances was explored in various QDs with variation of the finger gate electrostatic potential [5–10] to demonstrate the occurrence of the BSCs. An external magnetic field piercing QDs or Aharonov–Bohm rings was considered as an alternative physical parameter to achieve the BSCs [11–14]. An equivalent explication of the BSCs is that a degeneracy of the bound states of the same symmetry occurs under a variation of the QD parameter. Then the state superposed from two degenerate QD states can be decoupled from the continuum [5, 10].

When we deal with electron ballistic transport in quantum wires the number of continua is doubled because of the electron spin

$$E_\mu = \frac{\hbar^2}{2m}k_{\sigma_z}^2 - g^*\mu_B H_0\sigma_z \tag{1}$$

with the corresponding propagating states (continua)

$$\psi_\uparrow = \begin{pmatrix}1\\0\end{pmatrix}e^{ik_\uparrow x},\ \psi_\downarrow = \begin{pmatrix}0\\1\end{pmatrix}e^{ik_\downarrow x}. \tag{2}$$

However as long as the spin–orbit interaction is disregarded the Hamiltonian is decomposed into two decoupled blocks. Then the Friedrich–Wintgen mechanism for the BSC can be independently applied to each block giving rise to BSCs with definite spin projection due to the Zeeman term [15]. Account

of the spin–orbit interaction does not change the number of continua (2) however the spin dependent subsystems are coupled through the spin–orbit interaction. In that case the Friedrich–Wintgen mechanism of destructive interference of two resonances has to be reexamined with inclusion of all spin dependent continua whose number becomes equal to four when only the first propagation subband of both attached waveguides is open.

First, the problem of the BSC residing in a finite number of continua was considered by Pavlov-Verevkin and co authors [16, 17] in the framework of the Weisskopf–Wigner model [18, 19]. Rigorous statement about the BSCs was formulated as follows. The interference among N degenerate states which decay into K non-interacting continua generally leads to the formation of $N-K$ BSCs. The equivalent point of view is that the linear superposition of the N degenerate eigenstates $\sum_{n=1}^{N} a_n\psi_n$ can be achieved to have zero coupling with K different continua in $N-K$ ways by a variation of the N superposition coefficients a_n. Respectively, these coefficients a_n define an expansion of the BSC over the eigenstates of the closed QD. Note, that the number of continua is growing because of many physical reasons, for example, a few non symmetrically attached waveguides, multiple propagation subbands in the waveguides, or two polarizations of the radiation continuum in case of electromagnetic BSCs. Each case puts the problem of constructing BSCs on the line of art [7, 20–23].

In this paper we apply the above consideration to the open Aharonov–Bohm ring in the presence of the Rashba spin–orbit interaction (RSOI). As seen from figure 1 we have two waveguides and each of those have two spin dependent continua resulting in $K=4$. Nevertheless because of the symmetry relative to inversion $\mathbf{x}\to-\mathbf{x}$ it is sufficient to establish orthogonality of the superposed state $\sum_{n=1}^{N} a_n\psi_n$ with two spin polarized continua of only one waveguide. Therefore the number of continua is reduced effectively twice $K=2$ which requires a degeneracy of, at least, three eigenstates of the closed ring to realize BSCs. Thus, the BSC in the ring with the RSOI is a product of destructive interference of three resonant states. The threefold degeneracy of eigenstates can be achieved by continuous variation of two physical parameters, the magnetic flux and the RSOI strength. The last parameter is affected by external electric field [24]. The magnetic flux and the confinement potential which defines the size of the ring can be also chosen as an alternative pair of parameters.

Quantum rings made of semiconducting materials exhibiting RSOI have attracted considerable attention due to fundamental spin-dependent quantum interference phenomena that are observable in these systems. Since the strength of the RSOI can be tuned with external gate voltages [24], quantum rings or systems of them have possible spintronic applications. Aharonov–Bohm oscillations in the presence of SOI were observed in [25, 26] and systematic analysis of the conductance and polarization of transport electrons through the two-dimensional rings with the RSOI was presented by Nowak *et al* [27]. The electron transfer through quantum rings involves both the spin precession due to the RSOI and the quantum interference effects related to Aharonov–Bohm and

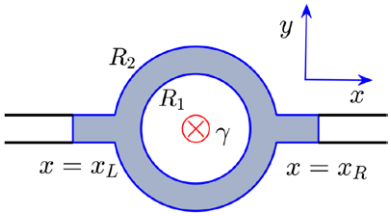

Figure 1. Aharonov–Bohm ring pierced by magnetic flux γ with two symmetrically attached waveguides. Shaded area indicates the region where the RSOI is present.

Aharonov–Casher (AC) effects [28, 29]. The latter spin-interference effect [30, 31] results from the fact that the relative phase shifts for the wave function passing through both arms of the ring are spin dependent in the presence of RSOI. So far numerous theoretical works have mostly addressed 1d rings [32–40]. This approach allows to obtain analytical description of charge and spin transport through the ring as function of the electron Fermi energy and the RSOI strength. Theoretical studies concerning 2d channels show however that for an accurate description of transport through the RSOI ring, the finite width of the channels can not be neglected [31, 41]. This is mainly due to the fact that for a finite-width ring the spin projection is no longer well defined [27, 41].

2. One-dimensional ring

The Hamiltonian of the 2d ring has the following form

$$\widehat{H}=\frac{\hbar^2}{2m^*}(-\mathrm{i}\nabla-\frac{e}{c\hbar}\vec{A})^2-\alpha[\vec{\sigma}\times(-\mathrm{i}\nabla-\frac{e}{c\hbar}\vec{A})]_z+\frac{1}{2}g^*\mu_{\mathrm{B}}H_0\sigma_z. \tag{3}$$

If radial modes of the 2d ring are neglected, one can use the one-dimensional Hamiltonian written as follows in a dimensionless form [32–40]

$$\widehat{H}=\left(-\mathrm{i}\frac{\partial}{\partial\varphi}+\frac{\beta}{2}\hat{\sigma}_r-\gamma\right)^2+\nu\,\gamma\hat{\sigma}_z \tag{4}$$

where $\gamma=\frac{\Phi}{\Phi_0}$ is the dimensionless flux piercing the 1d ring of radius R, $\beta=2\alpha\mathrm{Rm}^*/\hbar^2$ is the dimensionless RSOI constant, $\hat{\sigma}_r=\cos\varphi\hat{\sigma}_x+\sin\varphi\hat{\sigma}_y$, $\nu=2\pi g^*m^*/m$. $\Phi=\pi H_0R^2, \Phi_0=\hbar/e$ and H_0 is the external magnetic field. The Bohr magneton is absorbed by $\nu\gamma$. The Zeeman contribution in (4) is usually small $\nu\ll1$ [35]. Therefore, at the first step we can disregard this contribution. Then the eigenenergies of the 1d closed ring are [34–36, 38, 39]

$$E_{m\sigma}=(m+\gamma_{\mathrm{AC}}^{\sigma}-\gamma)^2, \tag{5}$$

where

$$\gamma_{\mathrm{AC}}^{\sigma}=\frac{1}{2}(1-\sigma\sqrt{1+\beta^2}) \tag{6}$$

is the spin dependent Aharonov–Casher flux [35] with $\sigma=\pm1$. The corresponding eigenfunctions are

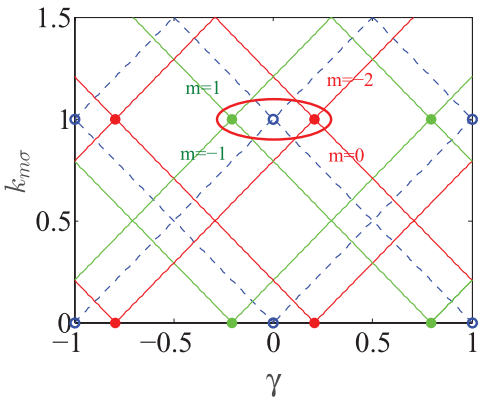

Figure 2. Eigenenergies $k_{m,\sigma} = \sqrt{E_{m,\sigma}}$ of closed 1d ring versus magnetic flux γ for $\nu = 0$. Dash lines corresponding to $\beta = 0$ are split when $\beta = 1$ (solid lines). The BSC points are marked by open circles at $\beta = 0$ and spin polarized BSCs are marked by closed circles.

$$\Psi_{m,+}(\varphi) = e^{im\varphi}\begin{pmatrix}\cos(\theta/2)\\ e^{i\varphi}\sin(\theta/2)\end{pmatrix},$$
$$\Psi_{m,-}(\varphi) = e^{im\varphi}\begin{pmatrix}\sin(\theta/2)\\ -e^{i\varphi}\cos(\theta/2)\end{pmatrix},$$
$$\tan\theta = -\beta. \tag{7}$$

The eigenenergies double degenerate in σ for $\beta = 0$ (dash blue lines in figure 2) are split in the presence of the RSOI (solid green lines for $\sigma = 1$) and (solid red lines for $\sigma = -1$).

As it was discussed in the Introduction BSCs occur at the degeneracy points in the spectrum of the closed ring. Let us show that not every degeneracy point corresponds to a BSC. The degeneracy occurs at the points: $E_{m\sigma} = E_{n\sigma'}$. First, we consider the case of the same spin projection $\sigma = \sigma'$. Then the degeneracy points are given by

$$\gamma - \gamma^{\sigma}_{\rm AC} = \frac{m+n}{2}. \tag{8}$$

At these points we have from equation (5)

$$E_{m\sigma} = E_{n\sigma} = \frac{(m-n)^2}{4}. \tag{9}$$

The necessary and sufficient condition for a BSC is that the coupling between the attached wires and the superposed degenerate states equals zero [14, 42]. That condition is achieved if the superposed state has nodal points at the points of wires attachment $\varphi = 0,\ \pi$. As a result we obtain for the BSC in the 1d ring

$$\Psi_{\rm BSC,+}(\varphi) = e^{i(m+n)\varphi/2}\sin(k\varphi)\begin{pmatrix}\cos(\theta/2)\\ e^{i\varphi}\sin(\theta/2)\end{pmatrix}, \tag{10}$$

and

$$\Psi_{\rm BSC,-}(\varphi) = e^{i(m+n)\varphi/2}\sin(k\varphi)\begin{pmatrix}-\sin(\theta/2)\\ e^{i\varphi}\cos(\theta/2)\end{pmatrix}, \tag{11}$$

where $k = (m-n)/2$ has to be integer. Thus the BSC occurs at crossing points of $E_{m,\sigma}$ and $E_{n,\sigma}$ where $m = n + 2k$ and equation (8) are both fulfilled. These BSC points are shown in figure 2 by closed circles. It is worthy noting that in the parametric space of the RSOI strength and flux the BSCs belong to lines defined by equation (8). For $\beta \to 0$ they limit to the BSC points at the integer values of the flux [14] shown in figure 2 by open circles. One can see from figure 2 that the BSC points are split by the RSOI in σ [38]. Therefore an electron with a definite spin projection can be trapped in the 1d ring with RSOI at discrete values of the flux defined by equation (8).

At the discrete values of the RSOI strength and flux

$$\sqrt{1+\beta^2} = 2m,\ m = 1, 2, 3, \ldots, \gamma = n + 1/2,$$
$$n = 0, \pm1, \pm2, \ldots \tag{12}$$

$$\sqrt{1+\beta^2} = 2m + 1,\ \gamma_n = n. \tag{13}$$

the spin polarized BSCs become degenerate. As it will be shown below the BSCs with account of the Zeeman term in the ring are close to the points given by equation (12) while the points defined by equation (13) have no relevance because of different symmetry of the eigenstates relative to the $\mathbf{x} \to -\mathbf{x}$.

Consider now the degeneracy of the eigenstates (7) with the opposite spin projections. At the degeneracy point the superposed wave function has the following form

$$\Psi = A\Psi_{m,+} + B\Psi_{n,-} = Ae^{im\varphi}\begin{pmatrix}\cos(\theta/2)\\ e^{i\varphi}\sin(\theta/2)\end{pmatrix} + Be^{in\varphi}\begin{pmatrix}\sin(\theta/2)\\ -e^{i\varphi}\cos(\theta/2)\end{pmatrix}. \tag{14}$$

One can instantly see that the condition $\Psi(0) = \Psi(\pi) = 0$ for the BSCs is never fulfilled.

The BSC point is the singular point where the unit conductance coalesces with the zero conductance [5, 14], i.e. a collapse of the Fano resonance occurs [46]. This has been already observed by Citro *et al* [39, 40]. It is also interesting to resolve the features of the spin polarization given by the relation

$$P = \frac{T_{\uparrow\uparrow} + T_{\uparrow\downarrow} - T_{\downarrow\uparrow} - T_{\downarrow\downarrow}}{T_{\uparrow\uparrow} + T_{\uparrow\downarrow} + T_{\downarrow\uparrow} + T_{\downarrow\downarrow}}. \tag{15}$$

where $T_{\mu,\nu}$ are the spin resolved transmission amplitudes. In the basis of the ring eigenstates (10) and (11) $T_{\mu,\nu}$ becomes diagonal [35, 39]

$$P = \frac{\sum_\sigma \sigma T_\sigma}{\sum_\sigma T_\sigma} \tag{16}$$

where the diagonal components of the transmission amplitudes were derived in [35]

$$T_\sigma = \frac{8i\cos[\pi(\gamma^\sigma_{\rm AC} - \gamma)]\sin\pi kR}{1 - 5\cos 2\pi kR + 4i\sin 2\pi kR + 4\cos[\pi(\gamma^\sigma_{\rm AC} - \gamma)]}. \tag{17}$$

Figure 3 shows the transmission amplitudes and polarization versus the Fermi wave number k and magnetic flux γ for both BSCs at $\beta = 1$ outlined by red oval in figure 2. Figures 3(a) and (b) show spin resolved transmission probabilities which demonstrate a collapse of the Fano resonance at the corresponding spin polarized BSCs marked by open

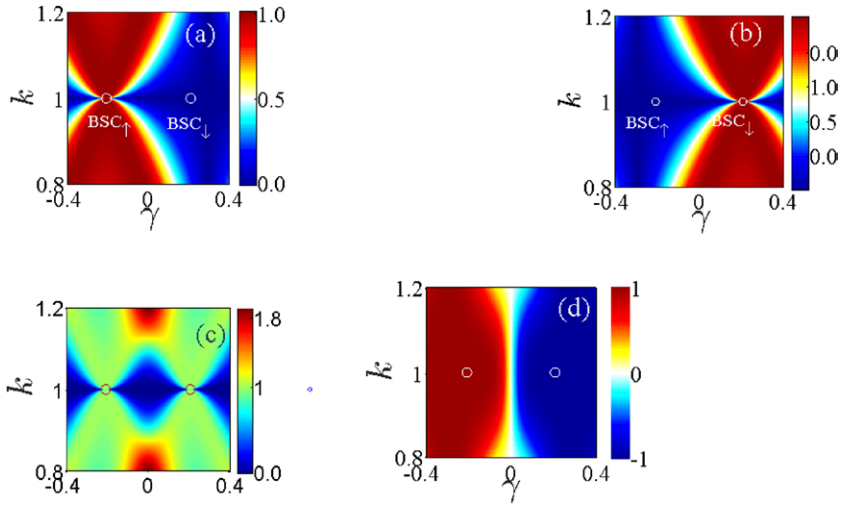

Figure 3. Spin resolved transmission probabilities T_+ (a) and T_- (b), total transmission (c) , and spin polarization (16) (d) versus flux and the Fermi wave number in the vicinity of the spin polarized BSCs outlined by oval in figure 2 for $\beta = 1$. The BSC points are marked by open circles.

circles. Respectively, the total transmission in figure 3(c) accumulates these features at both BSCs. Figure 3(d) demonstrates that in the vicinity of each spin polarized BSCs the spin polarization (15) of transmitted electrons attains its maximal value. In figure 4 shows the behavior of the poles of the transmission amplitudes (17). The points where the imaginary parts of the poles turn to zero exactly correspond to BSCs.

3. The effect of the Zeeman term

The Zeeman term in (4) modifies the eigenenergies and eigenfunctions of the 1d ring as follows [34, 36]

$$E_{m\sigma} = \frac{\beta^2}{4} + \left[m - \gamma + \frac{1}{2}\left(1 - \sigma\frac{1}{\cos\theta_m}\right)\right]^2 + \frac{1}{4}\left(1 - \frac{1}{\cos^2\theta_m}\right) + \frac{\nu\gamma\sigma}{\cos\theta_m}, \tag{18}$$

$$\Psi_{m,+}(\varphi) = e^{im\varphi}\begin{pmatrix}\cos(\theta_m/2)\\ e^{i\varphi}\sin(\theta_m/2)\end{pmatrix},$$
$$\Psi_{m,-}(\varphi) = e^{im\varphi}\begin{pmatrix}\sin(\theta_m/2)\\ -e^{i\varphi}\cos(\theta_m/2)\end{pmatrix}, \tag{19}$$

where

$$\tan\theta_m = -\beta\frac{m - \gamma + 1/2}{m - \gamma + 1/2 - \nu\gamma}. \tag{20}$$

The eigenenergies (18) are shown in figure 5(a). There are multiple degeneracy points for $m - n = 2k$. In order to find out whether they correspond to BSC with the superposed degenerate eigenfunctions (19) m, σ and n, σ' having nodal points at $\phi = 0, \pi$ we obtain the following equation

$$\tan\frac{\theta_m}{2} = \tan\frac{\theta_n}{2}, \sigma = \sigma',\ m \neq n \tag{21}$$

or

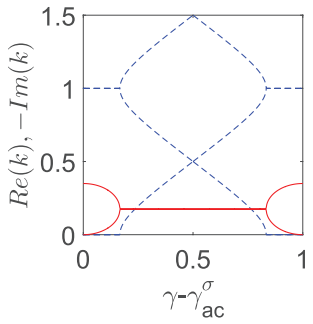

Figure 4. The resonant poles versus full flux $\gamma - \gamma^{\sigma}_{\rm AC}$ in accordance to (17). Dash lines show Re(k) and solid lines show Im(k).

$$\tan\frac{\theta_m}{2}\tan\frac{\theta_n}{2} = -1, \sigma = -\sigma'. \tag{22}$$

These equations are not compatible with the degeneracy condition $E_{m\sigma} = E_{n\sigma'}$. That result is in a full agreement with the arguments put forward in the Introduction that no BSC occurs in the Aharonov-Borm ring in the presence of the RSOI as a result of the twofold degeneracy for $\nu \neq 0$. However there could be BSCs resulting from threefold degeneracy of eigenstates of the same symmetry (18) as shown in figure 5(a). Then a linear superposition of three degenerate eigenfunctions satisfies the condition for the nodal points at $\phi = 0, \pi$.

Table 1 lists the values of the parameters at which threefold degeneracy occurs for $\nu = 0.2$. Effective electron g-factor g^*varies in a wide interval roughly from -10 to 10 as dependent on doping of the semiconductor material and the potential well which contains 2DEG [43, 44]. The effective electron mass can be of order of 0.1 m [44]. Respectively, the Zeeman term factor $\nu = 2\pi g^* m^*/m$ can vary from very small values to unit. Although in what follows we have chosen $\nu = 0.2$ this choice is not principal for the spin polarized BSCs. Note that we presented only those values of the parameters where the states of the same symmetry relative

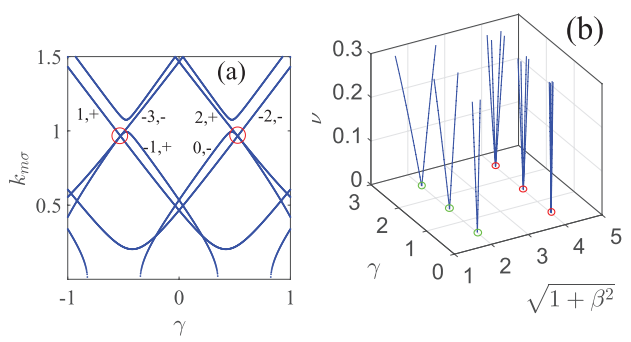

Figure 5. (a) Eigenenergies $k_{m\sigma} = \sqrt{E_{m\sigma}}$ of 1d ring versus the magnetic flux γ for $\nu = 0.2$, $\beta = 1.812$ (a). The open circles show the points indexed by 1 and 3 in table 1. (b) Lines of the threefold degeneracy in the space of physical parameters: flux, the RSOI strength and the Zeeman term factor ν in 1d ring with $k_{m\sigma}$ near by unit.

Table 1. Parameters of threefold degeneracy in the 1d ring with account of the Zeeman term $\nu = 0.2$.

Number of the BSC	k	β	γ	m	σ
1	0.965	1.812	0.526	0	−1
				2	+1
				−2	−1
2	1.035	1.651	0.526	0	1
				2	+1
				−2	−1
3	1.987	1.760	0.512	3	1
				−3	−1
				1	−1
4	1.987	1.702	0.487	1	−1
				−1	+1
				−3	−1
5	2.012	1.759	0.488	−1	1
				3	1
				1	−1
6	2.013	1.701	0.513	−1	1
				−3	−1
				3	1
7	2.992	1.751	0.508	2	−1
				4	1
				−4	−1
8	2.992	1.712	0.492	2	−1
				−2	1
				−4	−1
9	3.008	1.750	0.492	2	−1
				−2	1
				4	1

to $x \to -x$ are triply degenerate to give rise to BSCs in the vicinity of $\sqrt{1+\beta^2} = 2$ and $\gamma = 1/2$. There are also BSCs in the vicinity of points $\sqrt{1+\beta^2} = 2m, m = 1, 2, 3, \ldots$ and $\gamma = 1/2 + n, n = 0, \pm 1, \pm 2, \pm 3, \ldots$. Moreover in the three dimensional space of the flux, RSOI strength and giromagnetic ratio ν there are multiple lines with threefold degeneracy as shown in figure 5(c). These lines originate from the points given by equation (12) where the 1d ring has a fourfold degeneracy and respectively we have BSCs degenerate in spin when $\nu = 0$. With $\nu \neq 0$ each line corresponds to a spin polarized BSC. It is important to note that there is a number of points of threefold degeneracy with different symmetry relative to $\mathbf{x} \to -\mathbf{x}$. However as it was discussed in the Introduction only the states with the same symmetry give rise to a BSC at the point of threefold degeneracy. Table 2 lists only the points of threefold degeneracy with either all even or all odd azimuthal quantum numbers.

The above results for the BSC points fully agree with the behavior of the poles of the scattering matrix derived by Yi *et al* [32] in the presence of the Zeeman term by use of Shapiro matrix [45]

$$\begin{pmatrix} a' \\ b' \\ c' \end{pmatrix} = \begin{pmatrix} -f-g & \sqrt{\epsilon} & \sqrt{\epsilon} \\ \sqrt{\epsilon} & f & g \\ \sqrt{\epsilon} & g & f \end{pmatrix} \begin{pmatrix} a \\ b \\ c \end{pmatrix}, \tag{23}$$

which links the outgoing (a', b', c') and ingoing amplitudes (a, b, c). Here $f = \pm(\sqrt{1-2\epsilon} - 1)/2$, and $g = \pm(\sqrt{1-2\epsilon} + 1)/2$ with $\epsilon \leqslant 1/2$ and ϵ as phenomenological parameter which depends on the way of connection of waveguides to ring.

Figure 6(a) shows the poles behavior under the effect of giromagnetic ratio ν when other parameters are tuned to the point $\beta = \sqrt{3}, \gamma = 1/2$ which is degenerate over spin according to equation (12) for $\nu = 0$. One can see that the Zeeman term split degenerate resonances linearly over ν. However what is more important these BSCs become quasi-BSCs with extremely small resonant widths $\sim\nu^4$. In the second case we tuned the parameters to BSC 3 and BSC 5 from table 1. As shown in figure 6(b) the resonant positions are split almost in the same linear way in the giromagnetic ratio ν as for the first case in figure 6(a). However the resonant width turns to zero at $\nu = 0.2$ demonstrating occurrence of true BSCs. Figures 6(c) and (d) demonstrate that the resonant widths turn to zero under variation of the relevant physical parameters. Figure 6(d) show also that there are the BSCs in vicinity of $\beta = \sqrt{4^2 - 1}$ which are not listed in table 1.

The BSC 1 and BSC 2 from table 1 occur at slightly different points in the parametric space and are shown in figures 7(a) and (b) respectively. Although they are indistinguishable in the angular behavior of the spinor components as shown in figures 7(a) and (b) they have opposite spin textures given by mean spin $\vec{\sigma}(\phi) = \langle\Psi(\phi)|\vec{\sigma}|\Psi(\phi)\rangle$. Here $\Psi(\phi)$ is the scattering wave function within the ring. Figure 8 shows the BSC 5 in accordance to table 1.

In the Friedrich–Wintgen scenario for the BSC emerging from double degeneracy of the eigenstates of a closed QD the conductance undergoes so called Fano resonance collapse in the vicinity of the singular BSC point [5, 14, 46]. It is interesting to follow these features in the present scenario of the full destructive interference of three resonances. Figure 9(a) demonstrates the same features of the Fano resonance collapse as in figure 3(a) in the absence of the Zeeman term related to singularity of the inverse of matrix $H_{\text{eff}} - E$

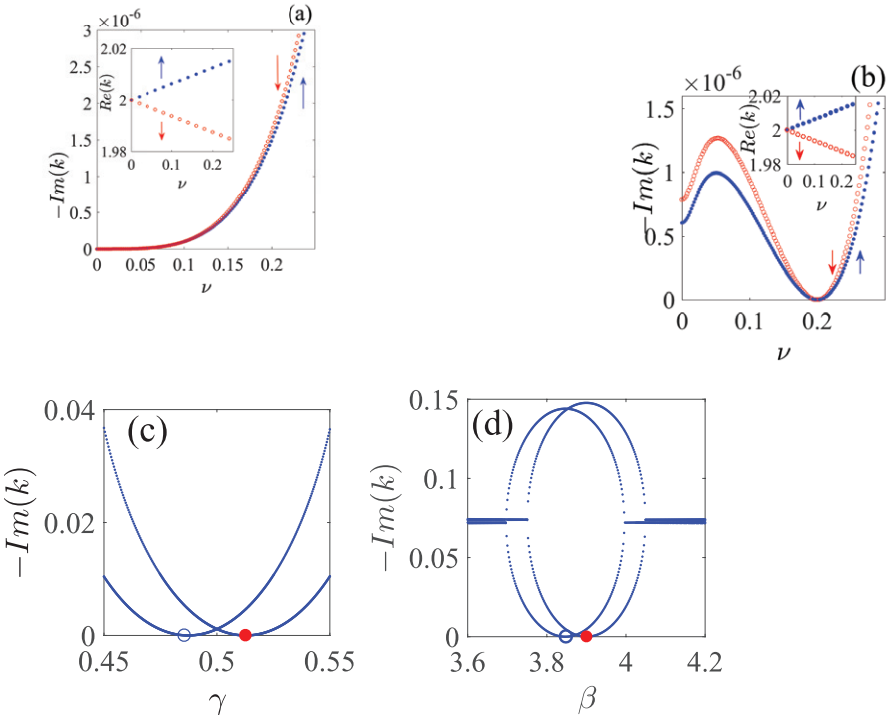

Figure 6. The poles versus ν for (a) $\gamma = 0.5, \beta = \sqrt{3}$ and (b) for the parameters tuned to the BSC 3 in table 1. Resonant widths versus (c) flux γ for $\beta = 1.76$ and (d) RSOI strength β for $\gamma = 0.512$. Open and closed circles mark the BSCs 3 and 4 spin polarized up and down, respectively.

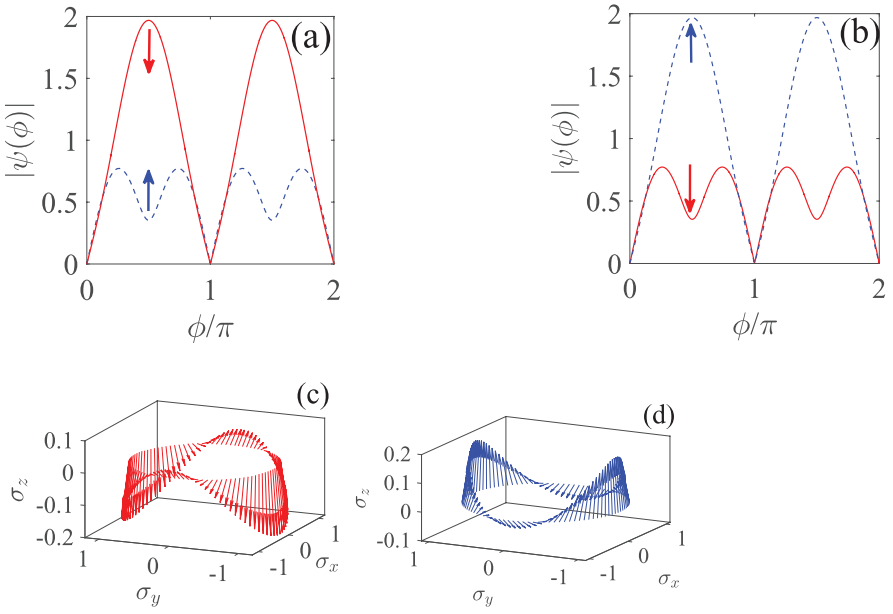

Figure 7. Profiles of the spinor components of BSCs 1 and 2 in accordance to table 1 marked in figure 6 by circles. (a) $\psi(\phi) = -1.0726\psi_{0,-} + \psi_{-2,-} + 0.366\psi_{2,+}$ and (b) $\psi(\phi) = -1.06\psi_{0,+} - 0.379\psi_{2,-} + \psi_{2,+}$. (c) and (d) the corresponding spin textures.

however with duplication of Fano features. It is important that each BSC point displays a singularity not only in the conductance but in the spin polarization which is maximal as shown in figure 9(b).

The spin textures in figures 7 and 8 show the evolution of the spin direction as the ring is encircled in ϕ similar to considerations in [31, 38, 41, 47–49, 51]. The textures are related to the geometric phase [51, 52]

$$\phi_g = \frac{\mathrm{i}}{\pi}\int_0^{2\pi} \Psi^+(\phi)\frac{\partial}{\partial\phi}\Psi(\phi)\mathrm{d}\phi, \tag{24}$$

where $\Psi(\phi)$ is the scattering wave function within the 1d ring. Such phase factors can be observed via interference of waves traversing different paths and were experimentally demonstrated in semiconductor quantum rings with RSOI [50, 53].

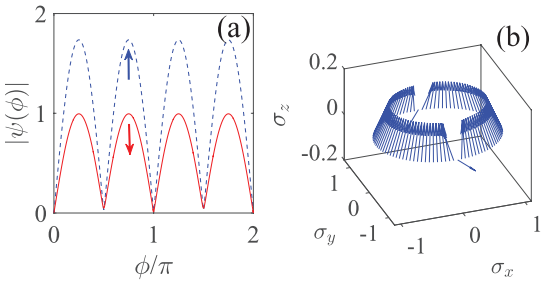

Figure 8. (a) Profiles of the spinor components of BSC 5 in accordance to table 1 $\psi(\phi) = -1.0007\psi_{-1,+} - 0.028\psi_{1,-} + \psi_{3,+}$. (b) Spin texture.

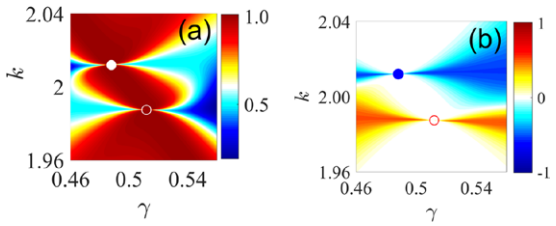

Figure 9. Conductance (a) and spin polarization (b) of the 1d ring versus flux and Fermi wave vector in the vicinity of two spin polarized BSCs (3 and 5 in table 1). The BSC points are marked by open and closed circles respectively.

Because the BSCs originate from the points of three-fold degeneracy in closed ring with account of the Zeeman term we also considered the variation of the geometric phase encircling the BSC point in the parametric space of flux γ and RSOI strength β. Following [14] we introduce the winding angle α

$$\gamma = \gamma_{\rm BSC} + r\cos\alpha,\ \beta = \beta_{\rm BSC} + r\sin\alpha \tag{25}$$

with the other parameters $k = k_{\rm BSC}$ and $\nu = 0.2$ tuned to the BSC point. Let us take BSC 1 in accordance to table 1. In figure 10(a) we show the evolution of transmission probability $T_{\sigma=1}$ and the spin texture within the ring for some selected values of angle α. One can see that the most noticeable transformations of the spin texture occurs close to the points $\phi = \pm 0$ or $\phi = \pi \pm 0$, where wires are attached to the ring. Respectively figure 10(b) presents the evolution of the mean spin close to these points. The most remarkable features are seen in figures 10(c) and (d) for the geometrical phase (24). One can see that the spin polarization (15) correlates with the geometric phase whose sharp changes evidence in favor of topological transitions as it was observed by Saarikoski *et al* [52].

4. Two-dimensional rings

The BSCs in 2d rings without RSOI were shown to exist in the vicinity of twofold degeneracy of the ring eigenstates with $m - n = 2k, k = 1, 2, 3, \ldots$ for integer values of the flux $\gamma = 0, \pm 1, \pm 2, \ldots$ where m, n are the azimuthal quantum numbers [14]. We show in this section that the BSCs occur in the 2d ring in the presence of the RSOI and the Zeeman term due to threefold degeneracy similar to the 1d ring. At first we present results of numerical computations of the conductance which evidence that spin polarized BSCs exist in 2d rings. Similar to the 1d ring in the presence of the Zeeman term these BSCs with different energies occur for the magnetic flux $\gamma \approx 1/2 + n$ and the RSOI strength β around the quantized values $\sqrt{(2m)^2 - 1}$, where $m = 1, 2, 3, \ldots$. In what follows we consider a 2d ring of mean radius $R = (R_1 + R_2)/2 = 2.5d$ (see figure 1) where d is the width of the waveguides.

An unambiguous tool for analysis of BSCs is the effective non Hermitian Hamiltonian [3–5, 16] obtained by the Feshbach projection of the total Hamiltonian onto the inner states of the QD [18]. In the approximation of infinite propagation band the effective Hamiltonian takes the Wigner–Weisskopf form [16, 54–56]

$$\widehat{H}_{\rm eff} = \widehat{H}_{\rm B} - {\rm i}\widehat{W}\widehat{W}^{+} \tag{26}$$

where the $\widehat{W}$ is $N \times M$ coupling matrix between M propagating channels of waveguides and N eigenstates of the ring. The matrix elements of $\widehat{W}$ are given by overlapping integrals [57, 58]

$$W^{C}_{b,p} = \int_0^d {\rm d}y \frac{\partial}{\partial x}\psi_b(x,y)\psi_p(x,y)\Big|_{x=x_C} \tag{27}$$

where $x_{\rm C}$ defines the position of the ring-waveguide interface (see the geometry of the open ring in figure 1), b enumerates the eigenstates which are coupled with the continua enumerated by index p of the Cth waveguide. In our case we have to account for the following. (i) Waveguides of finite width d with the Zeeman term have the following subbands

$$E_{\rm F} = k^2_{p\mu}R^2 + (\pi pR/d)^2 - \gamma\nu\mu, p = 1, 2, 3, \ldots \tag{28}$$

where the dimensionless Fermi energy is measured in terms of $E_0 = \hbar^2/2m^*R^2$. In what follows we assume that the electron propagates in the first subband. (ii) The indexes of the effective Hamiltonian and the coupling matrix besides the azimuthal quantum number also include the spin variable $\sigma = \pm$. Therefore we have the spin dependent effective Hamiltonian [57, 59]

$$\langle m\sigma|H_{\rm eff}|n\sigma'\rangle = E_{m\sigma}\delta_{mn}\delta_{\sigma\sigma'} - \sum_p \sum_{C=L,R} \sum_\mu W^{Cp\mu}_{m\sigma}(W^{Cp\mu}_{n\sigma'})^* {\rm e}^{{\rm i}k_{p\mu}a_0}, \tag{29}$$

which provides a tool for numerical analysis of the BSCs and conductance in the 2d open rings. Here the exponential factors $\exp({\rm i}k_p a_0)$ are a result of a finite subband width in the finite difference method with dispersion relation

$$E_{\rm F} = [4 - 2\cos k_p a_0 - 2\cos(\pi p/N_W + 1)]/a_0^2,$$

where $a_0 = d/N_W$ is the lattice unit in the discretized lattice with N_W points along the cross section of the waveguide [57, 59].

The conductance is given by the trace of the transmission amplitudes $G = Sp(TT^{+})$ given by the inverse of the effective Hamiltonian (29) [57]

$$T_{\mu\mu'} = \sum_{mn,\sigma\sigma'} (W^{L1\mu}_{m\sigma})^* \langle m\sigma| \frac{1}{\widehat{H}_{\rm eff} - E} |n\sigma'\rangle W^{R1\mu'}_{n\sigma'} \tag{30}$$

for propagation in the first channel $p = 1$. The results of calculations are collected in figure 11. Figure 11(a) shows

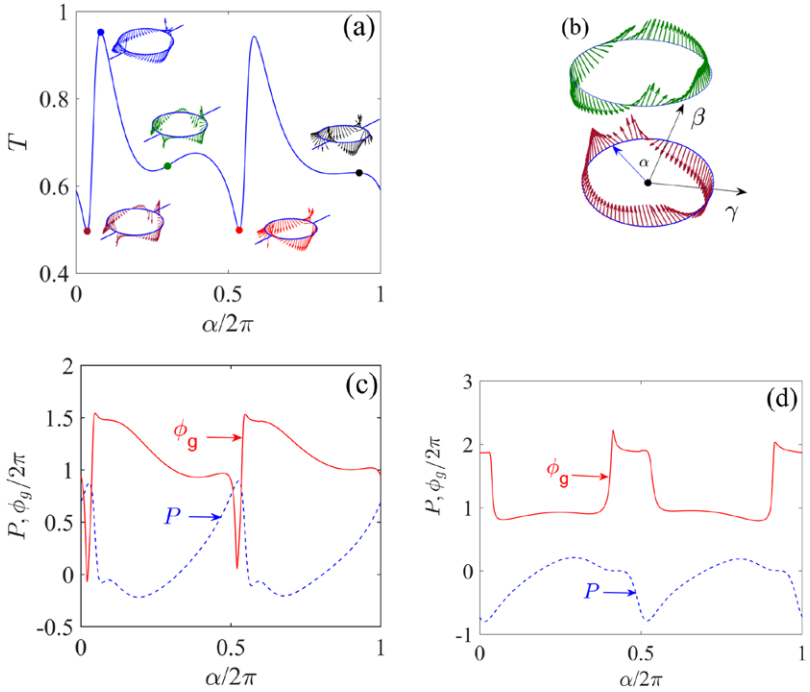

Figure 10. (a) Transmission probability $T_{\sigma=1}$ and spin textures of 1d ring and (b) $\vec{\sigma}(\phi = 0.1)$ (upper green arrows) and $\vec{\sigma}(\phi = -0.1)$ (bottom brown arrows) for encircling BSC 1 in the plane of parameters γ and β given by equation (25) with $r = 0.02$. Geometric phase and spin polarization (24) versus the angle of encircling (c) the BSC 1 point and (d) the BSC 2 point.

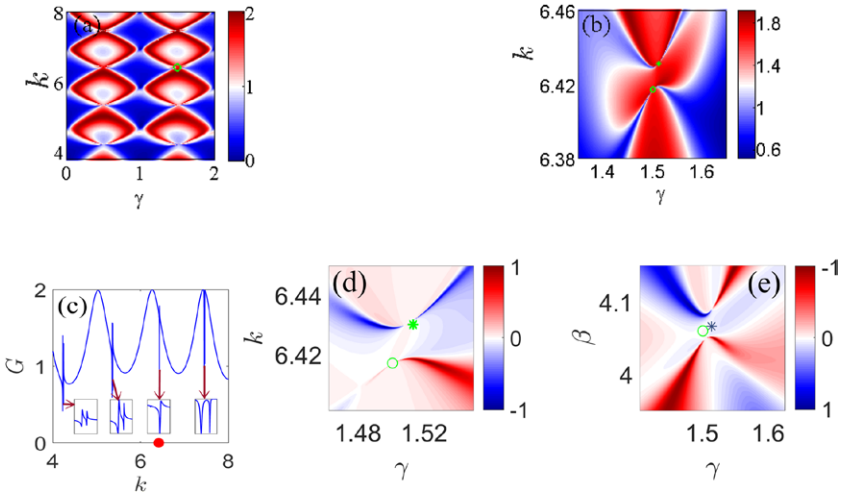

Figure 11. (a) and (b) Conductance of the 2d ring versus flux and Fermi wave vector of injecting electron. (c) The conductance versus Fermi wave number k. (d) Spin polarization versus k and γ. In all cases the parameters $\beta = 4.0598, \nu = 0.2$ are tuned to the 3th BSC point in accordance to table 2. (e) Spin polarization versus γ and β at $k = 6.4206$ in the vicinity of the pair of BSCs 1 and 2.

the conductance versus the flux and the Fermi wave number $k = \sqrt{E_F - \pi^2}$.

The conductance demonstrates a mass of narrow Fano resonant features similar to those calculated by Nowak *et al* [27]. When the parameters are tuned to BSC point $\beta = 1.761, \nu = 0.2$ given in table 2 these features are doubled as shown in the insets in figures 11(b) and (c). Figure 11(d) demonstrates that in the vicinity of each pair of the BSCs the electron flows have opposite spin polarizations. The third inset in figure 11(c) precisely shows that one of the features transforms into the collapse of Fano resonance. This is a result of the BSC when the inverse of the matrix $\widehat{H}_{\text{eff}} - E$ does not exists for $E = E_{\text{BSC}}$ giving rise to a singular behavior of the transmission amplitudes as seen from equation (30) [5]. Therefore the BSC point marked by open circle in figure 11(a) can be observed in the conductance. Zoomed figures 11(b) and (d) show that there are two BSCs split due to the Zeeman term. But only the BSC marked by open circle is true BSC 3 from table 2 while the second point marked by star corresponds to a quasi-BSC which becomes true BSC 4 if the RSOI constant is slightly adjusted according to table 2 similarly to the 1d ring. The radial spin σ_r is not preserved [41]. Therefore we specify the split BSCs by mean spin projection $\langle\sigma_z\rangle$. Figure 11(e) shows that spin polarization can be switched

Table 2. Parameters of threefold degeneracy of the eigenstates of the 2d ring with the mean radius $R/d = 2.5$ and the Zeeman term $\nu = 0.2$ occurs.

Number of the BSC	kR	β	γ	$\langle\sigma_z\rangle$
1	2.9249	1.7611	0.5102	0.47
2	2.9524	1.7159	0.4905	−0.496
3	6.4169	4.0598	1.501	0.161
4	6.4292	4.0662	1.514	−0.16
5	6.9112	1.7095	1.5221	0.475

by minor variation of magnetic field (flux γ) or electric field (the RSOI constant β). That that could have applications in spintronics.

Rigorously speaking we have $K = 4$ continua labelled as $L\uparrow, R\uparrow, L\downarrow$, and $R\downarrow$. However the inversion symmetry reduces the number of continua twice. So that for an arbitrary eigenstate we have

$$\begin{pmatrix} a(\mathbf{x}) \\ b(\mathbf{x}) \end{pmatrix} = (-1)^m \begin{pmatrix} a(-\mathbf{x}) \\ -b(-\mathbf{x}) \end{pmatrix}. \tag{31}$$

The coupling matrix elements are specified by two group of indexes, the indexes given by eigenstates of the closed ring $m, \sigma, \sigma = \pm$ and propagating modes of the waveguides given by $p = 1, \mu = \uparrow\downarrow$. With account of the symmetry rules (31) the fragment of the coupling matrix including four eigenstates of the ring $m, \pm$ and $n, \pm$ and four continua $C = L, R, \mu = \uparrow, \downarrow$ can be written as follows

$$\widehat{W} = \begin{pmatrix} W^{L\uparrow}_{m_1\sigma_1} & (-1)^{m_1} W^{L\uparrow}_{m_1\sigma_1} & W^{L\downarrow}_{m_1\sigma_1} & (-1)^{m_1+1} W^{L\downarrow}_{m_1\sigma_1} \\ W^{L\uparrow}_{m_2\sigma_2} & (-1)^{m_2} W^{L\uparrow}_{m_2\sigma_2} & W^{L\downarrow}_{m_2\sigma_2} & (-1)^{m_2+1} W^{L\downarrow}_{m_2\sigma_2} \\ W^{L\uparrow}_{m_3\sigma_3} & (-1)^{m_3} W^{L\uparrow}_{m_3\sigma_3} & W^{L\downarrow}_{m_3\sigma_3} & (-1)^{m_3+1} W^{L\downarrow}_{m_3\sigma_3} \\ W^{L\uparrow}_{m_4\sigma_4} & (-1)^{m_4} W^{L\uparrow}_{m_4\sigma_4} & W^{L\downarrow}_{m_4\sigma_4} & (-1)^{m_4+1} W^{L\downarrow}_{m_4\sigma_4} \end{pmatrix}. \tag{32}$$

The rank of the matrix (32) equals two if all m_j are either even or odd only. It may appear that similar to the 1d ring the BSCs in the 2d case are a result of the threefold degeneracy of the eigenstates of the closed ring. However there is important difference between the cases. First, as seen from equation (29) there are two contributions from the coupling with the continua, the anti-Hermitian part similar to equation (26) and the Hermitian part which gives rise to radiation shifts of eigenenergies of the closed 2d ring. Second, there are evanescent contributions to the Hermitian part of the effective Hamiltonian from the propagating subbands with $p > 1$:

$$\widehat{T} = \sum_{\mu} \sum_{\mu} \sum_{p>1} W^{Cp\mu}_{m\sigma} W^{Cp\mu}_{n\sigma'} \mathrm{e}^{-|k_{p\mu}|a_0}. \tag{33}$$

Assume now that there is a null eigenvector O of the coupling matrix with the open channel $\widehat{W}^{+}_{p=1} O = 0$. Then the necessary and sufficient condition for the BSC is

$$\widehat{H}_{\mathrm{eff}} O = (\widehat{H}_{\mathrm{B}} + \widehat{T}(E_{\mathrm{BSC}}))O = E_{\mathrm{BSC}} O.$$

If there were no contribution $\widehat{T}(E)$, the BSC would have occurred at the points of threefold degeneracy as it was in the 1d ring. In the 2d ring due to the exponentially small contribution of the closed channels $\widehat{T}(E)$ the BSC points are slightly shifted relative to the points of the exact threefold degeneracy. That effect is similar to the 2d ring without RSOI where the BSC points were shifted relative to the points of twofold degeneracy [14]. Moreover the evanescent modes give rise to an exponentially small extension of the BSCs into the waveguides as seen from figure 13.

Because of the energy dependence of the effective Hamiltonian the positions and widths of the resonance states are defined by the following nonlinear fixed point equations [56]

$$E_\lambda = \mathrm{Re}(z_\lambda(E_\lambda)),\ 2\Gamma_\lambda = -\mathrm{Im}(z_\lambda(E_\lambda)). \tag{34}$$

Here z_λ are the complex eigenvalues of the effective Hamiltonian (29) $\widehat{H}_{\mathrm{eff}}|\lambda) = z_\lambda|\lambda)$ with right eigenstates $|\lambda)$. The eigenfunction of the effective Hamiltonian (29) in the case $\mathrm{Im}(z) = 0$ gives the shape of the spin-polarized BSCs.

Figure 12 shows typical evolution of one of the solutions of equation (34) with the variation of the flux γ while other parameters of the ring were fixed at BSCs 3 and 4 according to table 2. The inset in figure shows that only one of these solutions with $\langle\sigma_z\rangle = 0.15$ is a true BSC when the parameters are tuned to BSC 3 while the second solution is a quasi-BSC with extremely small resonant width. Respectively, if the parameters are tuned to BSC 4 with negative spin polarization $\langle\sigma_z\rangle = -0.15$ the first solution becomes a quasi-BSC. Figures 12(b) and (c) evidence the existence of BSCs in the vicinity of the quantized values of the RSOI strength defined by equation (12) derived for the 1d ring.

The shapes of BSCs 3 and 4 are shown in figure 13.

5. Summary and discussion

In the absence of the RSOI the Hamiltonian of the Aharonov–Bohm ring is decomposed into two uncoupled subblocks. The number of continua in each subsystem equals the number of waveguides. Nevertheless for symmetrically attached identical waveguides as shown in figure 1 the number of continua effectively equals one provided that the Fermi energy of conducting electrons resides in the first propagating subband. Then spin dependent BSCs can occur by the Friedrich–Wintgen mechanism [3–5] of avoided crossing of two neighboring resonances originated from two degenerate eigenstates of the closed ring. If the Zeeman term is neglected the BSCs are degenerate in spin projection while the Zeeman term lifts the degeneracy. To switch spin polarization of the BSCs it is necessary to invert the external magnetic field.

The RSOI couples the spin dependent subsystems and therefore the total number of continua in the open ring becomes equal two. Then as it was discussed in the Introduction the number of resonances participating in the full destructive interference has to be increased, at least, to three. That in turn implies a threefold degeneracy of eigenstates of the closed 1d ring classified by the azimuthal quantum number m and spin σ given by equations (7). Patterns of such BSCs and their spin textures are shown in figures 7 and 8. The most remarkable

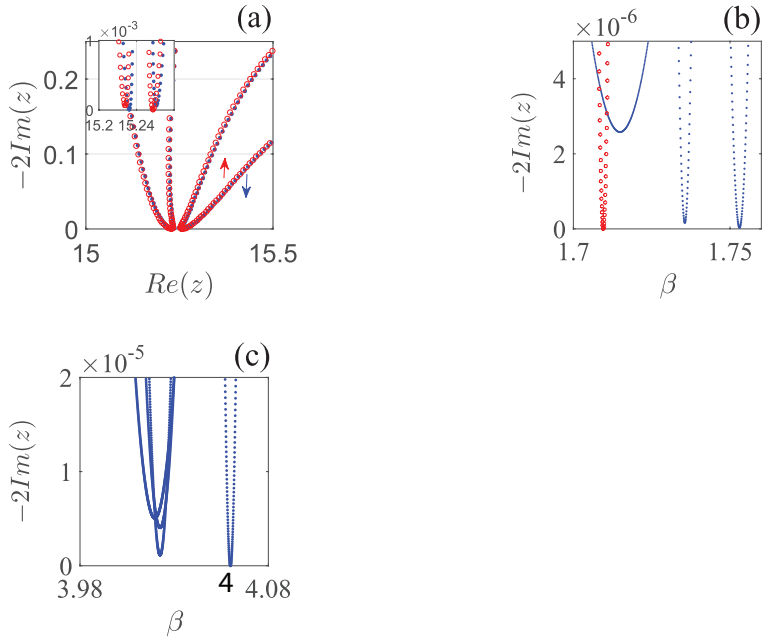

Figure 12. (a) Evolution of the resonance width $-2\mathrm{Im}(z)$ and resonance position $\mathrm{Re}(z)$ with the flux γ at $\beta = 4.0598$ (BSC 3 in table 2, red open circles) and $\beta = 4.0662$ (BSC 4, blue closed circles). (b) Evolution of the resonance width $-2\mathrm{Im}(z)$ with β at $\gamma = 0.5102$ (1th BSC, the blue closed circles) and $\gamma = 0.4905$ (2th BSC, the red open circles). (c) The same as in (b) but $\gamma = 1.501$ (3th BSC, the blue closed circles).

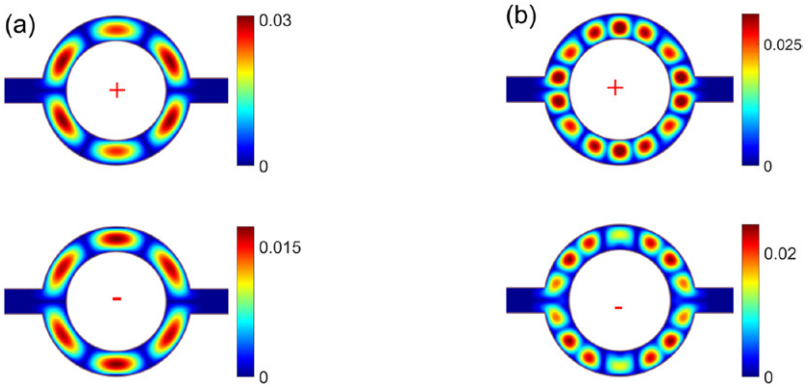

Figure 13. Shapes of BSC 1 (a) and BSC 2 (b) in accordance to table 2.

feature of these BSCs is that they occur in pairs with opposite spin projections as illustrated in figures 7(a) and (b). Some examples of the 2d BSCs are presented in figure 13. Noticeably they are located in the parametric space very close to each other. That paves a way for manipulation of spin in the Aharonov–Bohm ring with the RSOI. The points of threefold degeneracy can be easily found in the parametric space of the flux and the RSOI strength for the specific semiconductor interface with specific giromagnetic ratio ν. In three dimensional space of γ, β and ν there are multiple lines of the threefold degeneracy which originate from the points of fourfold degeneracy of the 1d ring without Zeeman term defined by equation (12). It is also important to note that the BSCs in the Aharonov–Bohm ring in the presence of the RSOI occur at half-integer flux in contrast to the rings without the RSOI.

Surprisingly, in the 1d ring in the presence of the RSOI but without of the Zeeman term the BSCs occur at the points of twofold degeneracy where the Weisskopf–Wigner model (26) is exact. Substitution of the ring states (7) into the coupling matrix (32) gives us

$$\widehat{W} = \begin{pmatrix} \cos\frac{\theta}{2} & \mathrm{e}^{\mathrm{i}\pi m}\cos\frac{\theta}{2} & \sin\frac{\theta}{2} & \mathrm{e}^{\mathrm{i}\pi m}\sin\frac{\theta}{2} \\ \cos\frac{\theta}{2} & \mathrm{e}^{\mathrm{i}\pi n}\cos\frac{\theta}{2} & \sin\frac{\theta}{2} & \mathrm{e}^{\mathrm{i}\pi n}\sin\frac{\theta}{2} \end{pmatrix}. \tag{35}$$

If $m - n = 2k,\ k = 1, 2, 3, \ldots$ then we obtain from (35) that

$$\widehat{W}\widehat{W}^{+} = 2\begin{pmatrix} 1 & 1 \\ 1 & 1 \end{pmatrix}. \tag{36}$$

One can see that in this case the rank of matrix $\widehat{W}$ and respectively $\widehat{W}\widehat{W}^{+}$ equals unit. Therefore according to [17] the twofold degeneracy of the closed system gives rise to a BSC. If the Zeeman term is included the coupling matrix modifies as follows according to equation (19)

$$\widehat{W} = \begin{pmatrix} \cos\frac{\theta_m}{2} & e^{i\pi m}\cos\frac{\theta_m}{2} & \sin\frac{\theta_m}{2} & e^{i\pi m}\sin\frac{\theta_m}{2} \\ \cos\frac{\theta_n}{2} & e^{i\pi n}\cos\frac{\theta_n}{2} & \sin\frac{\theta_n}{2} & e^{i\pi n}\sin\frac{\theta_n}{2} \end{pmatrix} \quad (37)$$

with the rank equal to two. Therefore it is necessary to have a threefold degeneracy of the eigenstates of the closed system to realize a BSC in the open system.

Numerics for the 2d Aharonov–Bohm ring has shown BSCs similar to those predicted for the 1d case. Although there are two points which make a difference between the cases: (i) exponential tails of BSCs in the attached waveguides due to coupling to the evanescent modes. (ii) the BSCs are positioned in the points of the parametric space β and γ slightly different from the points of threefold degeneracy of the closed 2d ring. Experimentally the BSC points can be achieved by tuning external fields: magnetic field which pierces the ring and electric field which affects the RSOI constant [24]. Importantly, the spin polarization of localized electron can be switched by a slight variation of the electric or magnetic field. A possibility to capture in the BSCs a conducting electron with a definite spin polarization opens new perspectives in spintronics.

Because the BSCs originate from the points of three-fold degeneracy in the closed ring we also considered the geometric phase encircling the BSC point in the parametric space of flux γ and RSOI strength β. Figure 10(a) demonstrates that the spin texture is sensitive to the encircling angle *alpha* in the close vicinity of the points where waveguides are attached to the ring as demonstrated in figure 10(b). Respectively one could expect the sudden changes in spin textures for small radius of encircling similar to those observed by Saarikoski *et al* [52]. Indeed consideration of the geometric phase versus the angle of encircling around the BSC point in space of flux and the RSOI strength for small radius of encircling r in equation (25) shows sharp changes.

Acknowledgments

This work has been supported by Russian Science Foundation through grant 14-12-00266. We acknowledge discussions with D N Maksimov and K N Pichugin.

References

[1] von Neumann J and Wigner E 1929 *Phys. Z.* **30** 465
[2] Stillinger F H and Herrick D R 1975 *Phys. Rev.* A **11** 446
[3] Friedrich E and Wintgen D 1985 *Phys. Rev.* A **32** 3231
[4] Volya A and Zelevinsky V 2003 *Phys. Rev.* C **67** 054322
[5] Sadreev A F, Bulgakov E N and Rotter I 2006 *Phys. Rev.* B **73** 235342
[6] Valsson O, Tang C-S and Gudmundsson V 2008 *Phys. Rev.* B **78** 165318
[7] Bulgakov E and Sadreev A 2011 *Phys. Rev.* B **83** 235321
[8] Prodanović N, Milanović V, Ikonić Z, Indjin D and Harrison P 2013 *Phys. Lett.* A **377** 2177
[9] Hrebikova I, Jelinek L and Silveirinha M G 2015 *Phys. Rev.* B **92** 155303
[10] Sadreev A F, Maksimov D N and Pilipchuk A S 2015 *J. Phys.: Condens. Matter* **27** 295303
[11] Nöckel J U 1992 *Phys. Rev.* B **46** 15348
[12] Wunsch B and Chudnovskiy A 2003 *Phys. Rev.* B **68** 245317
[13] Orellana P A, Ladron de Guevara M L and Claro F 2004 *Phys. Rev.* B **70** 233315
[14] Bulgakov E N, Pichugin K N, Sadreev A F and Rotter I 2006 *JETP Lett.* **84** 430
[15] Ramos J P and Orellana P A 2014 *Physica* B **455** 66
[16] Pavlov-Verevkin V B 1988 *Phys. Lett.* A **129** 168
[17] Remacle F, Munster M, Pavlov-Verevkin V B and Desouter-Lecomte M 1990 *Phys. Lett.* A **145** 265
[18] Feshbach H 1958 *Ann. Phys.* **5** 357
Feshbach H 1962 *Ann. Phys.* **19** 287
[19] Mahaux C and Weidenmüller H A 1969 *Shell Model Approach in Nuclear Reactions* (Amsterdam: North Holland)
[20] Hsu C W, Zhen B, Lee J, Chua S-L, Johnson S G, Joannopoulos J D and Soljacic M 2013 *Nature* **499** 188
[21] Zhen B, Hsu C W, Lu L, Stone D and Soljačić M 2014 *Phys. Rev. Lett.* **113** 257401
[22] Yang Y, Peng C, Liang Y, Li Z and Noda S 2014 *Phys. Rev. Lett.* **113** 037401
[23] Bulgakov E N and Sadreev A F 2015 *Phys. Rev.* A **92** 023816
[24] Nitta J, Akazaki J T, Takayanagi H and Enoki T 1997 *Phys. Rev. Lett.* **78** 1335
[25] Nitta J, Meijer F, Narita Y and Takayanagi H 2000 *Physica* E **6** 318
[26] Grbić B, Leturcq R, Ihn T, Ensslin K, Reuter D and Wieck A D 2007 *Phys. Rev. Lett.* **99** 176803
[27] Nowak M P, Szafran B and Peeters F M 2011 *Phys. Rev.* B **84** 235319
[28] Capozza R, Giuliano D, Lucignano P and Tagliacozzo A 2005 *Phys. Rev. Lett.* **95** 226803
[29] Szafran B and Peeters F M 2005 *Phys. Rev.* B **72** 165301
[30] Nitta J, Meijer F E and Takayanagi H 1999 *Appl. Phys. Lett.* **75** 695
[31] Frustaglia D and Richter K 2004 *Phys. Rev.* B **69** 235310
[32] Yi Y-S, Qian T-Z and Su Z-B 1997 *Phys. Rev.* B **55** 10631
[33] Meijer F E, Morpurgo A F and Klapwijk T M 2002 *Phys. Rev.* B **66** 033107
[34] Splettstoesser J, Governale J M and Zülicke U 2003 *Phys. Rev.* B **68** 165341
[35] Molnar B, Peeters F M and Vasilopoulos P 2004 *Phys. Rev.* B **69** 155335
[36] Wang X F and Vasilopoulos P 2005 *Phys. Rev.* B **722** 165336
[37] Aeberhard U, Wakabayashi K and Sigrist M 2005 *Phys. Rev.* B **72** 075328
[38] Sheng J S and Chang K 2006 *Phys. Rev.* B **74** 235315
[39] Citro R, Romeo F and Marinaro M 2006 *Phys. Rev.* B **74** 115329
[40] Citro R and Romeo F 2007 *Phys. Rev.* B **75** 073306
[41] Bulgakov E N and Sadreev A F 2002 *Phys. Rev.* B **66** 075331
[42] Bulgakov E N, Rotter I and Sadreev A F 2007 *Phys. Rev.* A **75** 067401
[43] Kiselev A A, Ivchenko E L and Rossler U 1998 *Phys. Rev.* B **58** 16353
[44] Winkler R 2003 *Spin–Orbit Coupling Effects in Two-Dimensional Electron and Hole Systems* (*Springer Tracts in Modern Physics* vol 191) (Berlin: Springer)
[45] Shapiro B 1983 *Phys. Rev. Lett.* **50** 747
[46] Kim C S, Satanin A M, Joe Y S and Cosby R M 1999 *Phys. Rev.* B **60** 10962
[47] Hentschel M, Schomerus H, Frustaglia D and Richter K 2004 *Phys. Rev.* B **69** 155326
[48] Frustaglia F, Hentschel M and Richter K 2004 *Phys. Rev.* B **69** 155327
[49] Lopes-Oliveira V, Castelano L K, Marques G E, Ulloa S E and Lopez-Richard V 2015 *Phys. Rev.* B **92** 035441
[50] Nagasawa F, Takagi J, Kunihashi Y, Kohda M and Nitta J 2012 *Phys. Rev. Lett.* **108** 086801

[51] Nagasawa F, Frustaglia D, Saarikoski H, Richter K and Nitta J 2013 *Nat. Commun.* **4** 2526
[52] Saarikoski H, Vázquez-Lozano J E, Baltanás J P, Nagasawa F, Nitta J and Frustaglia D 2015 *Phys. Rev.* B **91** 241406
[53] Richter K 2012 *Physics* **5** 22
[54] Sokolov V V and Zelevinsky V G 1992 *Ann. Phys., NY* **216** 323
[55] Dittes F M 2000 *Phys. Rep.* **339** 215
[56] Okołowicz J, Płoszajczak M and Rotter I 2003 *Phys. Rep.* **374** 271
[57] Sadreev A F and Rotter I 2003 *J. Phys. A: Math. Gen.* **36** 11413
[58] Pichugin K, Schanz H and Seba P 2001 *Phys. Rev.* E **64** 056227
[59] Datta S 1995 *Electronic Transport in Mesoscopic Systems* (Cambridge: Cambridge University Press)